Hindawi
Advances in Materials Science and Engineering
Volume 2018, Article ID 3625053, 12 pages
https://doi.org/10.1155/2018/3625053

Research Article

Model Test of the Reinforcement of Surface Soil by Plant Roots under the Influence of Precipitation

Hengxing Wang,[1] **Yulong He**,[2] **Zufeng Shang**,[3] **Chunpeng Han**,[1] **and Yilu Wang**[1]

[1]*School of Civil Engineering, Northeast Forestry University, Harbin 150040, China*
[2]*School of Transportation, Jilin University, Changchun 130025, China*
[3]*University of New South Wales, Sydney, NSW 2052, Australia*

Correspondence should be addressed to Zufeng Shang; z5047315@ad.unsw.edu.au

Received 2 June 2018; Accepted 2 August 2018; Published 16 September 2018

Academic Editor: Mercedes Solla

We present the results of the reinforcement of plant root systems in surface soil in a model test to simulate actual precipitation conditions. In the test, *Eleusine indica* was selected as herbage to reinforce the soil. Based on the various moisture contents of plant roots in a pull-out test, a fitting formula describing the interfacial friction strength between the roots and soil and soil moisture content was obtained to explain the amount of slippage of the side slope during the process of rainfall. The experimental results showed that the root systems of plants successfully reinforced soil and stabilized the water content in the surface soil of a slope and that the occurrence time of landslides was delayed significantly in the grass-planting slope model. After the simulated rainfall started, the reinforcement effect of the plant roots changed. As the rainfall increased, the interfacial friction between the roots and the soil exhibited a negative power function relationship with the water content. These conclusions can be used as a reference for the design of plant slope protection and reinforcement.

1. Introduction

A slope landslide is a type of extensive geological disaster, and the most important and direct cause of landslides is rainfall [1, 2]. Previous studies have discussed extensively the mechanism of action of slope collapse under the conditions of rainfall, and multiple theories have been proposed. According to the distribution curve of the soil aperture, using statistical analysis theory, Fredlund et al. analysed the relationship between the substrate suction of unsaturated soils and water content [3]. Mariano et al. conducted a linear discriminant analysis to describe the relationship between rainfall and landslides in Bogotá, Colombia [4]; Salciarini et al. analysed the regional initiation of rainfall-induced shallow landslides in the eastern Umbria region of Central Italy [5]; and Domenico et al. used a complete methodology for deriving the critical threshold, starting from the creation of a reliable database of historical rainfall and landslide events occurring in Sicily (Italy) [6].

The physical and mechanical responses of soils during the landslide process are often analysed through simulation and model tests. Artificial rainfall model tests have been widely used in studies on soil slope landslides. The sliding deformation of soil slopes during the rainfall process can be observed intuitively, and physical parameters (such as the landslide displacement) can also be measured quantitatively through an artificial rainfall model test, which is a major research tool used to study landslide instability models. Li et al. analysed the effect of the inclined weak interlayers on the rainfall response of a bedded rock slope [7, 8]. In addition, Li et al. experimented with a model test study on a landslide of a reservoir bank near a dam following rainfall [9]. Regmi et al. indicated the possibility of finding a relationship between the rainfall intensity, sliding initiation time, and position of its slip surface head in a natural-slope failure-prone zone [10]. Luo et al. experimented with a model test study on landslides under rainfall and reservoir water fluctuations [11]. Pan et al. experimented with a model test of the rainfall warning criteria

of retrogressive landslides [12]. Ahmadi-adli et al. experimented with model tests on rainfall-triggered landslides in unsaturated soil [13]. Kim et al. studied the effect of seepage on shallow landslides, located in changes in topography, using a model test [14]. In most cases, slides on mountain slopes are caused primarily by the slip of surface soil. In engineering construction, plant slope protection technology is used widely as a reinforcement method. The principle of plant slope protection is concentrated in two aspects [15–19]: the reinforcement of plant roots to the soil slope and the antierosion effect of vegetation cover. Herbaceous plants are one of the most commonly used reinforcement plants and are often used in slope protection to enhance the slope stability and reduce the risk of landslides of the surface soil.

Burylo et al. studied the enhanced soil cohesion during early stages using six plant roots from the southern French Alps [20]. Voottipruex et al. studied the effect of a composite RR system (Soil Reinforcement with Combination Roots Systems) on slope stability [21]. Saifuddin and Osman found that white cephalosporins have root systems with excellent hydrodynamic properties and can strengthen the soil when planted along a slope [22]. Bischetti et al. experimented with tests on root strength and root area ratio in Lombardy (Northern Italy) [23]. Genet et al. analysed the influence of plant diversity on slope stability [24].

In the above studies, the slope slip model under the precipitation conditions was discussed in depth. However, the research on the slope slip model under the function of vegetation protection was not as comprehensive. By comparing model tests of slope reinforcement by plants during the rainfall process with slope model tests of the plain soil under the same conditions, the present study establishes that the plant reinforcement slope model has a superior antislip ability. Combined with a pull-out test of plant roots and soil under various moisture content conditions and the results of stretch testing, the effect of plant root systems on soil reinforcement was obtained during simulated rainfall.

2. Material and Methods

2.1. Experimental Material. *Eleusine indica* was selected as the experimental grass. Photographs of the plant of interest are shown in Figure 1. Tendon grass is an annual herbaceous plant that has a relatively developed root system and is an excellent soil-protecting plant. The experimental procedure is as follows: select the normal growth of plants in the field, enclose the plants in a fixed area, dig a sample soil column containing the root system along the boundary of the limited area with a soil cutter, test the root system of the plants obtained, use the electronic scale to measure the quality of soil samples and quality of the root system, and calculate the root-containing rate of soil samples, using the following equation:

$$P_r = \frac{m_0}{m_f}, \tag{1}$$

where P_r is the root-content rate, m_0 is the quality of dry roots in the soil sample, and m_f is the total mass of the soil sample.

The soil samples used in the experiment are subgrade soil from a road in Harbin. The colour of the soil body is light yellow, with a standard viscosity, and the type of soil is silty clay. Basic geotechnical experiments on the selected soil samples were conducted, and their basic physical and mechanical parameters were obtained by calculations, as shown in Table 1.

2.2. Scheme of the Model Test. To study the slip failure mode of shallow soil in slopes under the reinforcement of plant roots, a slope scale model was developed to record the displacement trend of surface soil under rainfall conditions. In addition, a same-dimensional plain soil model was tested under the same conditions to reflect the effect of plant reinforcement on the surface soil of the slope.

The model box, made of toughened glass and measuring 142 cm × 50 cm × 50 cm, was placed on a 50 cm × 50 cm toughened glass plate and separated into an independent cabinet of 50 cm × 50 cm × 50 cm. The model size of the slope is as follows: the bottom length was 50 cm, the top length was 20 cm, the width was 50 cm, the height was 30 cm, and the slope angle was 45 degrees. According to the model size, 80% compaction degree and 10% moisture content were taken as the initial conditions to weigh the corresponding mass of soil and water. The mixture was stirred to ensure sufficient compaction, and then, the 50 cm × 50 cm toughened glass plate was used to cut the slope. Artificial grass planting was conducted using the grass-soil slope model according to the actual measured root density. The displacement slider was arranged on the slope, and the displacement of the slider along the slope and the vertical slope was measured and recorded using a displacement metre. A gauge point at a height of every 7.5 cm on the axis of the slope was taken, and three gauge points were marked as A, B, and C. At each gauge point, two dial gauges are arranged and marked. The dial gauge along the slope was marked as No. 1, No. 2, and No. 3 from top to bottom, and the dial gauge along the vertical slope was marked as No. 4, No. 5, and No. 6 from top to bottom. The rainfall system was arranged and was controlled at 8 mm/h. To simulate possible loads at the top of the slope (i.e., artificial structures such as buildings and pavements), a weight of 30 kg was applied to the top of the slope. After the start of the test, the data were recorded when the displacement metre reading started to change. The displacement metre reading was recorded every 1 min. After a large slip occurred, when the displacement of the slider was less than 0.05 mm for 5 min continuously, the landslide was considered to have ended, and data recording was stopped. The experimental arrangement and the simulated rainfall device are shown in Figure 2.

2.3. Pull-Out Test. Since the interface friction between roots of *Eleusine indica* and the soil is unknown, there is a possibility that the root system in the soil is pulled off during the process of a pull-out test. Therefore, the pull-out test of plant root systems was conducted to measure the extreme tension value.

(a) (b)

Figure 1: Photographs of the plant of interest.

Table 1: Physical and mechanical parameters of the soil.

Liquid limit (%)	Plastic limit (%)	Plasticity index	Maximum dry density ($g \cdot cm^{-3}$)	Optimum moisture content (%)	Proportion
34.1	22.2	11.9	1.92	11.2	2.66

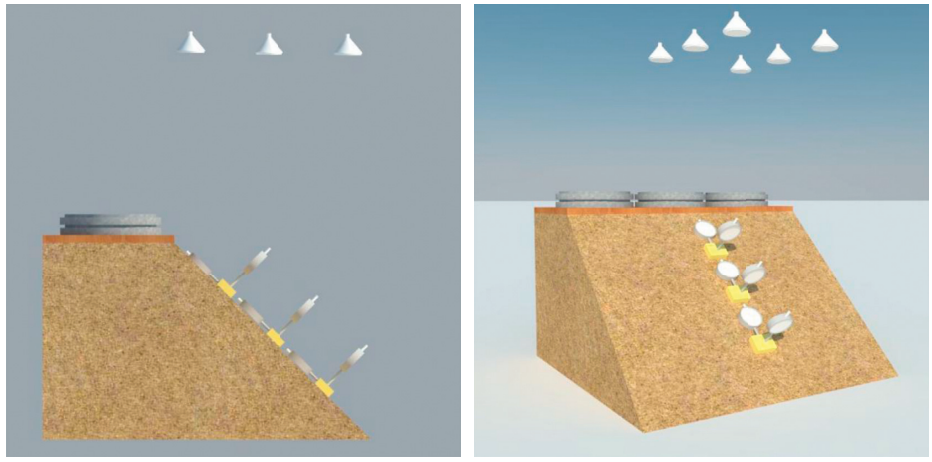

Figure 2: Test arrangement device.

2.3.1. Scheme of the Stretch Testing. Ten strains of *Eleusine indica* were selected randomly, and 5 pieces of intact rhizomes were screened randomly for each strain. A total of 50 plant rhizomes were used as the stretching materials. The average diameter, top diameter, and bottom diameter of the plant rhizomes were measured using a digital microscope. 50 plant rhizomes' histogram of diameter distribution is shown in Figure 3.

A digital force gauge with a force precision of 0.01 N (ZP-500, HK AIGU Instrument & Apparatus Co. Ltd., China) was used in the stretch testing to control the speed of tensile loading on reinforced soil. In this experiment, the tension rate was controlled to 0.16 mm/s. In the stretch testing, one end of the root system was fixed by an anchor, and the other end was fixed to the anchor of the force sensor. In the experiment, the rotation speed of the rocker

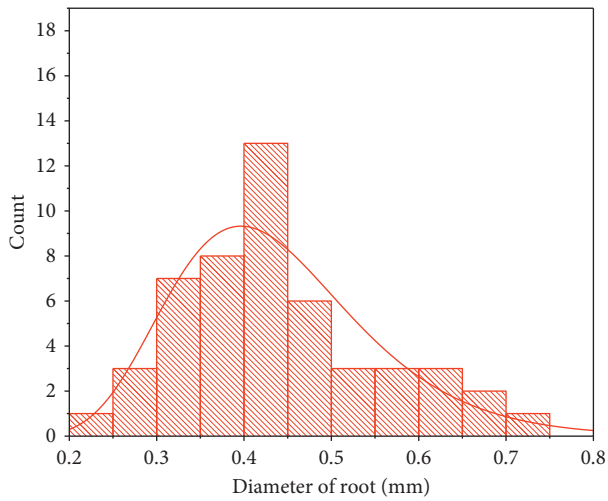

Figure 3: Distribution of the diameter of 50 rhizomes.

was controlled until the rhizome was pulled off, and then, the peak of the tension of the rhizome during the pulling test was recorded automatically using a computer terminal. The experimental process is shown in Figure 4.

2.3.2. Scheme of the Pull-Out Test. In the drawing experiment, the test pieces were prepared as follows: the roots of the plant selected on-site were washed clean and air-dried in the natural state. Root systems with a satisfactory shape and with a diameter close to the average were chosen. The middle of the plant roots was cut by 10 cm to provide spare samples.

According to a compaction degree of 80% and various moisture contents, namely, 10%, 11%, 12%, 13%, 14%, 15%, 16%, 17%, 18%, 19%, 20%, 21%, 22%, and 23%, a certain amount of water and drying soil was weighed and stirred evenly. The mixture was put in a container and sealed for 24 hours to ensure an even distribution of water content. Then, a vibratory hammer was used to compact the soil, and half of the mass of soil was placed in the sleeve. Subsequently, the plant roots, which were needed in the test, were threaded through the sleeve crevice. To simulate the situation that the root of an herbaceous plant was pulled out in the actual project, the thick end of the plant root was taken as the anchorage end. The end of the embedded segment was reserved for 10 mm and buried in the soil 61.8 mm deep, and the anchorage end was reserved for 28.2 mm. The remaining soil was poured into the sleeve and placed into the block, and then, the soil was formed using a vibratory hammer. The moulding specimen was a round pie-shaped specimen with a diameter of 61.8 mm and a height of 20 mm. To ensure the reliability of the test results, 3 parallel specimens were configured for each test piece. We took 3 times the standard deviation as the limit to remove the discrete points, took the average value of the test results, and used the test results which are close to the average value of the reliable test data as the analysis data. The single-root drawing experiment can be used to measure the interface friction between soil and plant roots and the changing trend of the friction of reinforced soil during the process of the pull-out test. The pull-out test of reinforced soil was conducted using a customized experimental instrument to control the speed of the pull-out test of the reinforced soil. Based on the results of the pull-out test, the mean value of the distribution corresponding to the diameter of the rhizome was chosen as the test diameter. The drawing rate was controlled to 0.16 mm/s, and the digital force gauge was consistent with the stretch testing. The size of the soil specimen was $61.8 \times 20\ \text{mm}^3$, as was the size of the direct shear specimen. During the pull-out test, the tension value of the plant rhizome was recorded automatically using the computer terminal, and the pulling curve was constructed. The experimental process is shown in Figure 5.

3. Results and Discussion

3.1. Model Test. According to the model experiment scheme, the displacement of the slide block was collected every 5 min; the results are shown in Figure 6.

The landslide process of the pure soil slope ended at 423 min, and the landslide process of the planting soil slope ended at 705 min, indicating that the implantation of a grass system can delay landslides. The landslide processes for the two types of slopes were roughly similar and can be divided into three stages: the slow slip stage, the severe slip stage, and the stop stage. In the slow sliding stage, all the slide blocks in the vertical slope had a tendency to bulge, and the amount of the change was approximately equal. This condition arose because the strength of the surface soil was maintained at the initial stage of the landslide. Under the action of the top pressure, the topsoil subsided vertically. Because of the restraint of the tempered glass at the bottom and the other three directions, the slope corresponds to the free boundary, which caused the uplift of the slope soil, and the displacement of soil along the slope was smaller. According to relevant research [25, 26], the soil moisture content changes occasionally during rainfall, and the wetting front advances along the vertical slope direction. At the beginning of rainfall, the rainfall infiltrates gradually along the slope, and the wetting front does not advance to the crack surface.

To further study the actual slip condition of the surface soil on the slope, the displacement value of the displacement metre in two directions is processed to obtain the total displacement value (Figure 7) and the total slip rate (Figure 8) of each measuring point. Each reaction volume is calculated as in the following equations:

$$s = \sqrt[2]{s_h^2 + s_n^2}, \tag{2}$$

$$v = \frac{ds}{dt}, \tag{3}$$

where s_h is the displacement along the slope and s_n is the displacement along the vertical slope.

Figure 7 shows that the implantation of the *Eleusine indica* effectively extended the time of the uniform speed

(a) (b)

Figure 4: Operating process of the pull-out experiment. (a) Diameter measuring. (b) Stretch testing.

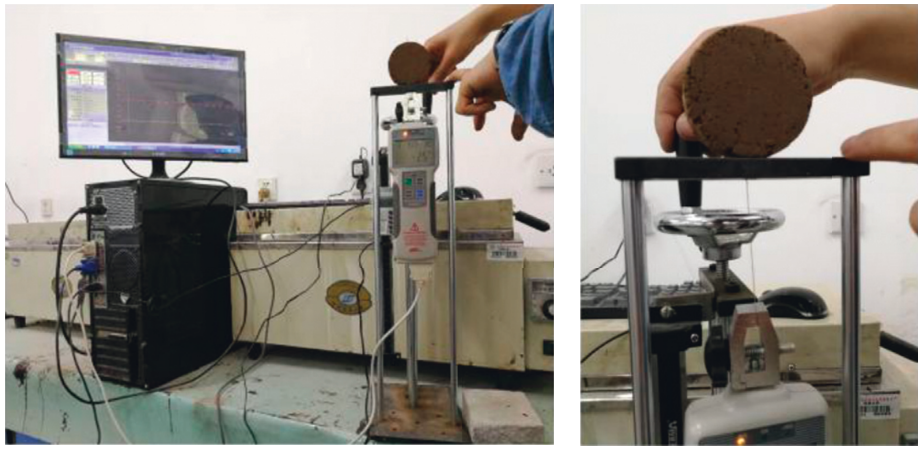

(a) (b)

Figure 5: Operating process of the pull-out experiment. (a). Digital force gauge. (b). Root drawing.

stage and acceleration stage of the landslide. In addition, the amount of slippage of the slope with plant roots was much smaller than that of the slope with pure soil. When the rainfall had just begun, since the rainwater was in a dynamic state in the surface soil, the soil inside the pure soil model remained in a dry state. Because the mechanical suction of the soil was larger, the rainfall infiltration exceeded the rainfall, and the water content of the surface soil did not rise sharply. Precipitation infiltration into the surface soil caused slope uplift and simultaneously triggered a partial pressure head of water. The appearance of a pressure head accelerated the infiltration of rainwater, leading to the continuous descent of the saturated zone of topsoil, making the self-weight of topsoil increase, and the shear strength of soil quickly declined. When the sliding force was greater than the antiskid force, a partial collapse landslide was initiated.

When the pure soil slope entered the accelerated slip stage, the wetting front reached the sliding surface of the soil mass; thus, the strength of the soil at the sliding surface decreased sharply, and the shallow soil slope presented an integral slip. During the process of instability, the rainfall increased continuously, the wetting front continued to move downward, and the increase in the water content of the upper soil led to an increase in the sliding force. Therefore, as the slip rate at this stage continued to increase, the slider displacement showed a nonlinear trend of growth. Due to the continuous infiltration of rainfall, the soil pressure on the

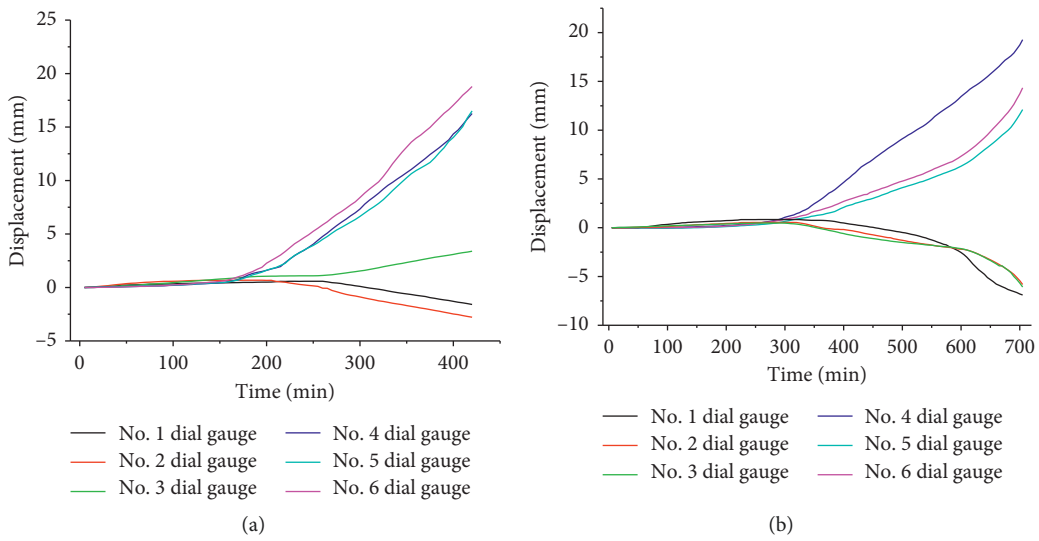

Figure 6: Results of the model test. (a) Pure soil. (b) Soil with plant.

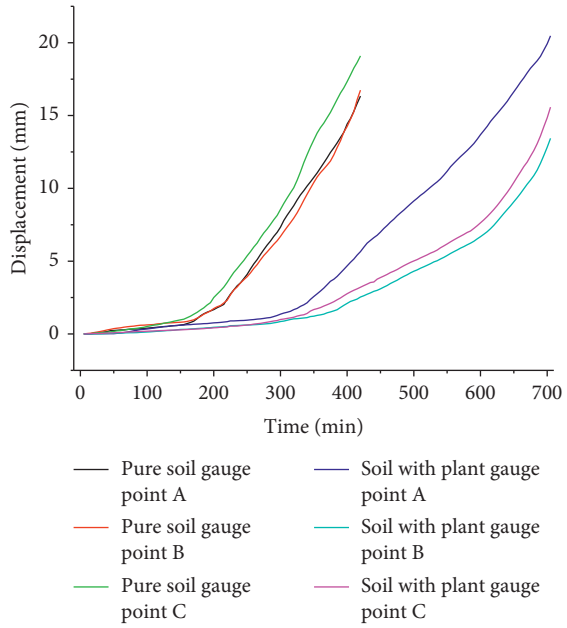

Figure 7: Total displacement value.

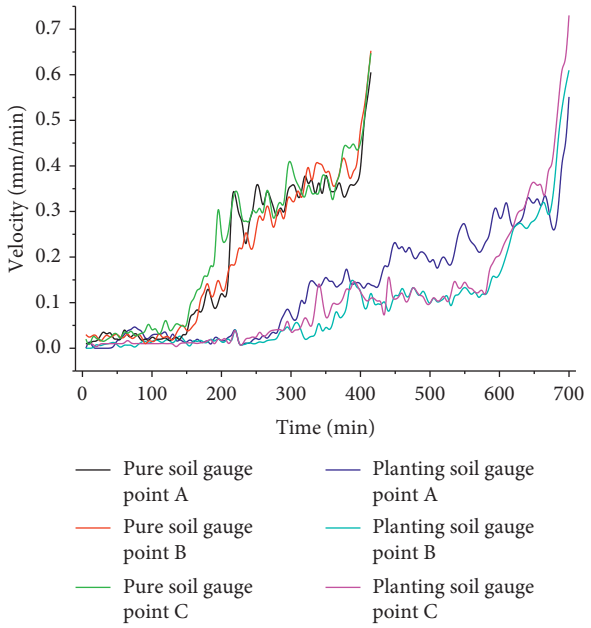

Figure 8: Total slip rate.

bottom of the slope gradually increased, and the soil of the upper slope pushed the soil of the lower slope so that the slippage of the bottom slider first appeared. The slippage of the bottom slide caused further slippage of the upper soil. Simultaneously, with increasing precipitation, the soil moisture content and the deformation of the inclined slope increased. Under the action of a vertical uniform load, the displacement of the top of the model slope was not uniform, and a crack appeared some distance from the slope, causing the slope angle to change greatly.

According to related research [27, 28], the landslide history of the two types of slopes can be divided according to the slip speed. As shown in Figure 8, during the precipitation process, the trend in the velocity change of the planting slope is much slower than that of the pure soil slope. However, the system still enters the stage of accelerated deformation because as the moisture content increases, the friction effect of reinforced soil keeps continually decreasing but retains some antislip ability. Furthermore, the root system of surface plants can play a role in antiscouring when the total amount of precipitation increases.

Figure 9(a) shows a perforative large crack when the slippage of the surface soil reaches a certain stage. At this time, the sliding speed at the bottom and central part of the pure soil slope changes sharply, and the slip displacement also increases sharply. Due to the small water content, the top slider has not yet reached the saturation of soil, and its sliding change rate is small. As shown in Figure 9(b), due to the reinforcement effect of rhizomes, when the total amount of rainfall continues to increase, with the slipping amount of the planting slope increasing continuously, the slip rate at the

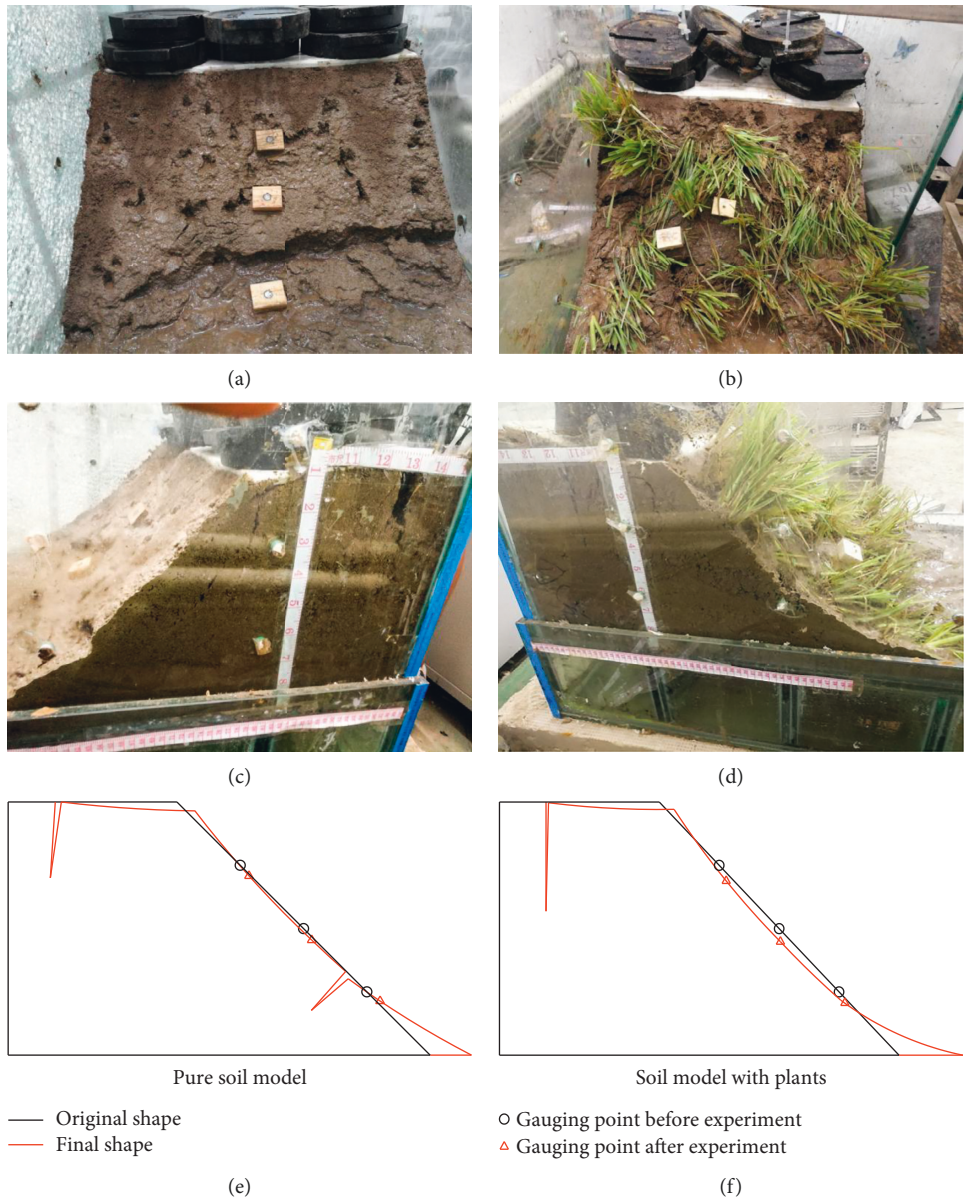

Figure 9: Destruction photos of the model test. (a). Surface destruction of the pure soil slope (b). Surface destruction of the planting slope. (c). Lateral destruction of the pure soil (d). Lateral destruction of the planting soil. (e). Destroyed side profile of the pure soil. (f). Destroyed side profile of the planting soil.

bottom is greater than the slip rate at the top. With increasing water content, the interfacial shear strength between plant rhizome and soil decreases gradually. When the amount of soil deformation at the bottom is too large, a small tensile crack appears on the surface of the slope. Although the reinforcement effect of a single plant rhizome on soil is not easily detectable, the net connection between rhizomes and plants still has a certain inhibitory effect on the tensile cracks. The slip rate of a slide at the bottom of the planting slope is smaller than that of the pure soil slope, resulting in a smaller final slip. According to the lateral photos of two different slopes after being destroyed, such as those shown in Figures 9(c) and 9(d), the final failure profiles can be drawn through the change in the displacement values of the measured points and the final destruction photos, as shown in Figures 9(e) and 9(f).

As shown in Figures 9(c), 9(d), 9(e), and 9(f), the slump mode of the two types of slopes under rainfall is essentially the same. When the slope of the pure soil is eventually destroyed, the slope angle rises outward, causing a large sliding deformation of the slide at the bottom and causing the slide of the slope to show a parallel downward trend along the slope. The slippage of the angle of the planting slope is large, the curve trend of the slope shows a trend of inward depression, and the trend in the depression on the upper slope is large.

To study the slope slippage form of planting slopes during the rainfall process, the slope angles of different slides should be discussed. Assuming that the slope is always in a straight line and that the continuity of the fracture surface is satisfactory before the fracture, a reasonable

theoretical model for calculating the slope angle is shown in Figure 10. The formula for calculating the slope angle at different positions on the slope is shown in Equation (4). The results are shown in Figure 11.

$$\sin\beta = \frac{l \cdot \sin\alpha - \sqrt{x^2 + y^2} \cdot \cos\left(\tan^{-1}(y/x) + \alpha\right)}{l}. \quad (4)$$

where α is the initial fracture angle (45°), β is the instantaneous slope angle, l is the slope length from the measuring point to the bottom of the slope, and (x, y) is the displacement of the measuring point.

As shown in Figure 11, no large-scale slippage of the soil occurs in the early stage of rainfall; thus, the change of the slope angle corresponding to each measuring point is small. With increasing soil slippage in the surface slope, the slope angle corresponding to each measuring point varies greatly. According to the theoretical calculation, the slope angle of each measuring point tends to change periodically, and at the final time point, the slope angle of the sliders is not substantially changed, which is clearly different from the actual slope type in Figure 9. This condition arises because in the process of a landslide, the deformation of the slope soil does not remain continuous; tension cracks arise that cause a significant change in the landslide angle.

On the destroyed slope, we took a small amount of soil from every 1 cm in the vertical direction from the top of the slope to the slope angle and measured its moisture content. The sampling points are shown in Figure 12. The trend map of the final distribution of water content of the two types of slopes along the height is shown in Figure 13.

The moisture content of the surface of the slope model increases with decreasing slope height. The difference in the water content between the top and the bottom of the pure soil model is 33%. The difference in the water content between the top and the bottom of the planting soil model is 18%, and the increasing trend in the latter is relatively gentle, implying that plant roots tend to balance the distribution of the water system in the surface soil. At a height of 1/3, an inflection point appears in the water content of the pure soil slope model, and the growth rate of the water content suddenly increases where the tension crack appears.

3.2. Results of Pull-Out Testing. According to Fukuda's theory [29], the effect of plant root reinforcement on soil depends mainly on the relationship between the tension (T) of roots and root and soil friction ($\Delta\tau$), as shown in Figure 14.

$$\begin{aligned}
\tau_1 &= \sigma\tan\varphi + c,\\
\tau_2 &= \frac{T\sin\beta}{A} + \sigma\tan\varphi + c = \frac{T\cos\beta}{A},\\
\Delta\tau &= \tau_2 - \tau_1 = \frac{T\sin\beta\tan\varphi}{A} + \frac{T\cos\beta}{A}\\
&= \frac{T\left(\sin\beta\tan\varphi + \cos\beta\right)}{A},
\end{aligned} \quad (5)$$

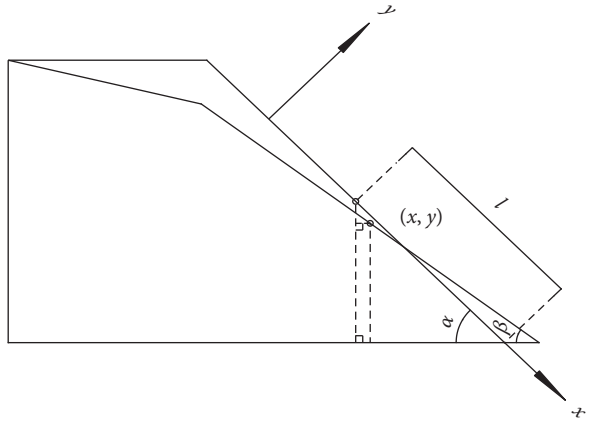

Figure 10: Theoretical slope angle calculation model.

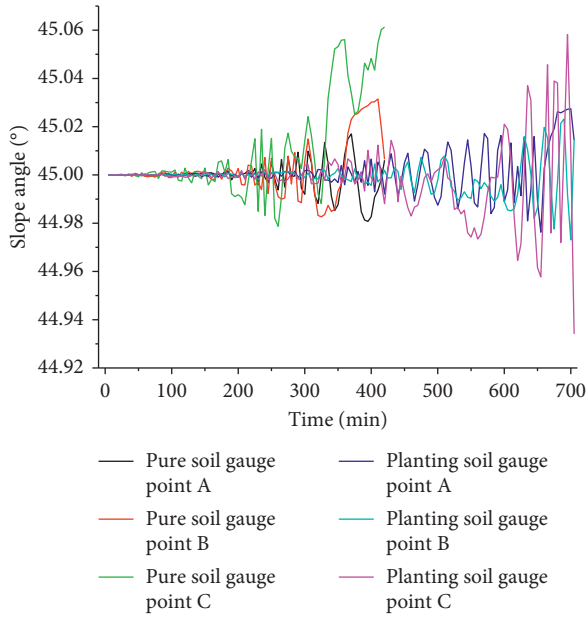

Figure 11: Changes in the slope angle.

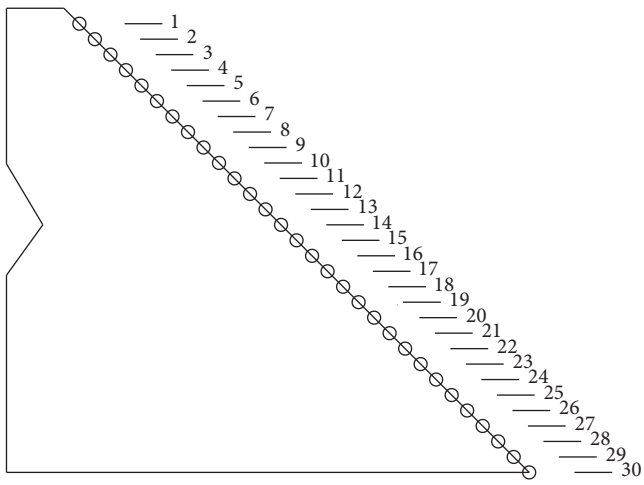

Figure 12: Sampling point of the moisture content.

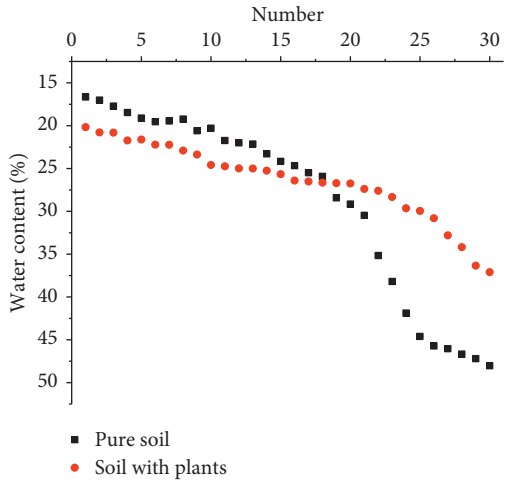

Figure 13: Moisture content.

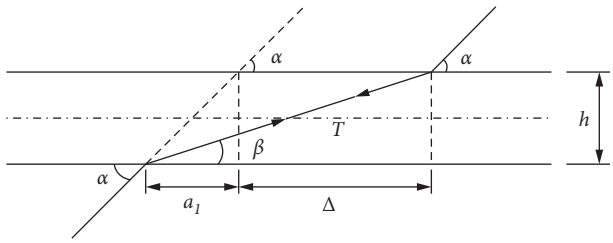

Figure 14: Force model of a single fibre under the shear action of a soil body.

where $\Delta\tau$ is the shear displacement, φ is the internal friction angle of soil, c is the cohesive of soil, and T is the tensile force of fibre.

There are two failure factors of root reinforcement: (1) if the interface friction between the soil and a root is large enough that tension on the root is greater than the root tensile strength, plant roots are pulled off, and (2) if the interface friction is small, roots are pulled from the soil instead of being pulled off. Thus, stretch testing is conducted to research the fracture factors of plant roots in the soil. Pull-out testing is conducted to characterize the interface friction effect between plant roots and soil for various moisture contents.

3.2.1. Results of Stretch Testing. Stretch testing was conducted according to previously published methods. The tensile strength changes in various diameters of *Eleusine indica* are shown in Figure 15.

A clear linear trend in plant rhizome diameter and its tensile strength is shown in Figure 15 (the adj. R-square value is 0.90921). The diameter of most plant root rhizomes is approximately 0.4 mm. We calculated the plant root rhizome diameter to be 0.4 ± 0.02 mm. Pull-out testing was conducted to research the effect of interface friction between roots and soil.

3.2.2. Results of Pull-Out Testing. The reinforcement effect between plant roots and soil at different moisture contents is different. To further study the interface friction effect of

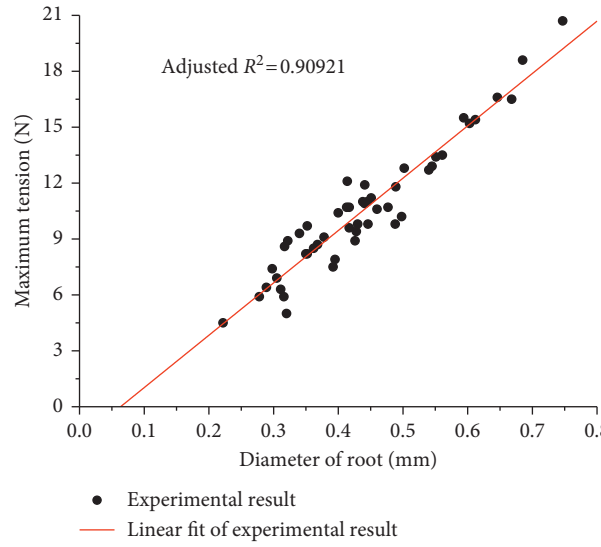

Figure 15: Result of stretching test.

root-soil and the failure mode of plant reinforcing topsoil, pull-out testing was conducted at various moisture contents, and the frictional force between roots of *Eleusine indica* and soil at various moisture contents was measured. The results are shown in Figure 16.

The tension curves of root-soil at different moisture contents show similarities, all of which appeared in four stages [30]: the elastic stage, the dynamic friction stage, the residual strength stage, and the resting stage. At the beginning of pull-out testing, due to the static friction between plant roots and soil, the tensile force value of plant roots increases rapidly and presents a linear trend. When the tensile force value of plant roots is equal to the maximum static friction between plant roots and soil, the tensile force value of plant roots reaches the maximum value, which is the interfacial shear strength between the plant roots and soil particles. When plant rhizomes begin to slide between soil particles, the static friction between plant roots and soil translates into dynamic friction. In the process of the continuous pulling of plant roots, soil particles and plant roots continue to reach a new equilibrium of friction. With the thicker part of plant roots being unplugged continuously, the tensile force value drops rapidly. When the plant roots are completely pulled out, the tension force value of the roots drops to 0.

The interfacial shear strength between plant roots and soil has a close relationship with the moisture content in soils: a greater soil moisture content corresponds to a smaller interfacial shear strength. The interfacial shear strength between plant roots and soil particles is determined mainly by three factors. When the soil moisture content increases, the friction coefficient between the plant roots and soil decreases, and then the shear strength of the interface decreases. To further explore the relationship between the soil moisture content and the interfacial shear strength of plant roots and soil, the interfacial shear strength of plant roots and soil at various moisture contents was fitted as shown in Figure 17. The reasonable fitting formula is proposed in the following equation:

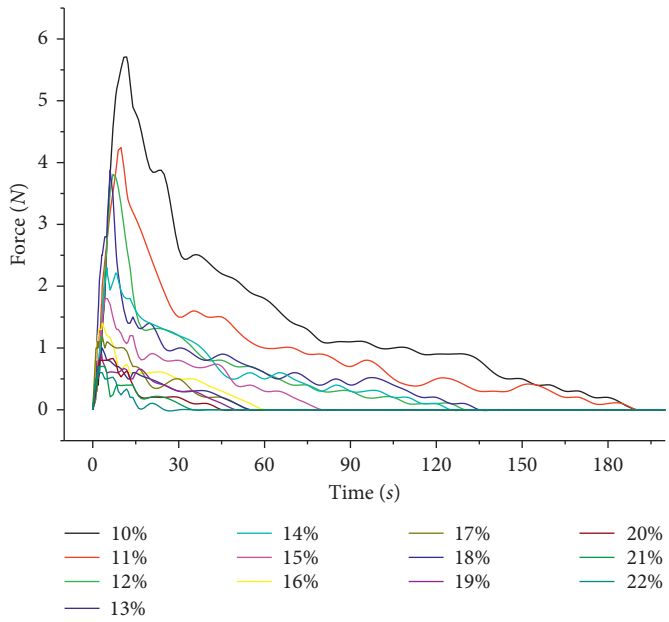

Figure 16: Results of pull-out testing.

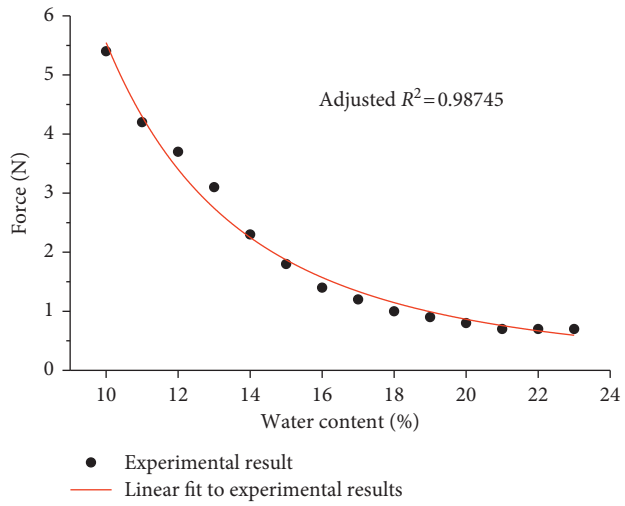

Figure 17: The maximum tensile force at different moisture contents.

$$y = 2670.06x^{-2.682}. \quad (6)$$

As shown in Figure 17, a clear negative power function on interface shear strength and moisture content can be obtained (the adj. R-square value is 0.90921). When the soil moisture content is 10%, the interfacial shear strength between roots and soil is larger, at 5.4 N. The interfacial shear strength decreases rapidly with increasing moisture content. When the soil moisture content reaches 20%, the interfacial shear strength between plant roots and soil is 0.8 N; thus, the interfacial shear strength has decreased by 85.19%. With increasing moisture content, the declining trend of interface shear strength is slow, and the effect of plant rhizome on soil reinforcement is relatively weak. We hypothesize that during rainfall, the plant root reinforcement effect for the topsoil is lost once the surface soil moisture content of the slope has dropped to a certain critical point, leading to the landslide of the surface soil of the slope.

As shown in Figures 15, 16, and 17, the ultimate tension of plant roots is generally above 6 N. However, at the minimum moisture content (10%), the interface between soil and roots is below 6 N. Therefore, we speculate that the main failure mode that causes root reinforcement during a landslide is the pull-out of the root system.

4. Conclusions

We researched the reinforcement of plant root systems to surface soil under the condition of precipitation. The major conclusions can be summarized as follows:

(1) The model test results show that three stages can be discerned in the landslides of the plain soil slope and the grass-soil slope: the first stage is the slow slip phase, the second is the uniform speed slip phase, and the third is the accelerating speed slip phase. According to the slope time, the landslide stages are greatly delayed by planting grass, and altering the slope rate and reinforcing the grass can effectively delay landslide occurrence and reduce the amount of slippage.

(2) According to the root pull-out test, the interfacial friction between the root and the soil exhibits a negative power function relationship with the water content. The friction effect between the soil and roots decreases rapidly with increasing soil moisture content.

(3) No plant roots are pulled off during the slipping of the plant slope; thus, the mechanism of the landslide is that the decline of the friction effect between the soil and roots from the increase in the soil moisture content reduces the strength of the root-soil complex. A landslide occurs once the sliding resistance is less than the sliding force, and the reinforcement effect of the roots also decreases during the landslide.

(4) When simulated rainfall ends, the surface water content distribution of the grass-soil slope is more uniform, but a gap exists in the surface water content distribution of the plain soil slope (33%). Thus, the study establishes that plant root systems are beneficial for stabilizing the surface soil water distribution.

Data Availability

The data used to support the findings of this study are available from the corresponding author upon request.

Conflicts of Interest

The authors declare that they have no conflicts of interest.

Acknowledgments

This work was supported by the Science and Technology Project of Heilongjiang Provincial Department of Transport, Fundamental Research Funds for the Central Universities (2572014CB21), and Natural Science Foundation of Heilongjiang Province in China (E201349).

References

[1] E. Garcia-Urquia and K. Axelsson, "The use of press data in the development of a database for rainfall-induced landslides in Tegucigalpa, Honduras, 1980–2005," *Natural Hazards*, vol. 73, no. 2, pp. 237–258, 2014.

[2] R. Mueller and S. Loew, "Predisposition and cause of the catastrophic landslides of August 2005 in Brienz (Switzerland)," *Swiss Journal of Geosciences*, vol. 102, no. 2, pp. 331–344, 2009.

[3] D. G. Fredlund and A. Xing, "Equations for the soil-water characteristic curve," *Canadian Geotechnical Journal*, vol. 31, no. 4, pp. 521–532, 1994.

[4] A. M. Ramos-Canon, L. F. Prada-Sarmiento, M. G. Trujillo-Vela, J. P. Macías, and A. C. Santos-R, "Linear discriminant analysis to describe the relationship between rainfall and landslides in Bogota, Colombia," *Landslides*, vol. 13, no. 4, pp. 671–681, 2016.

[5] D. Salciarini, J. W. Godt, W. Z. Savage, P. Conversini, R. L. Baum, and J. A. Michael, "Modeling regional initiation of rainfall-induced shallow landslides in the eastern Umbria Region of central Italy," *Landslides*, vol. 3, no. 3, pp. 181–194, 2006.

[6] D. Caracciolo, E. Arnone, F. Lo Conti, and L. V. Noto, "Exploiting historical rainfall and landslide data in a spatial database for the derivation of critical rainfall thresholds," *Environmental Earth Sciences*, vol. 76, no. 5, p. 222, 2017.

[7] L. Q. Li and N. P. Ju, "Effect of the inclined weak interlayers on the rainfall response of a bedded rock slope," *Journal of Mountain Science*, vol. 13, no. 9, pp. 1663–1674, 2016.

[8] L. Q. Li, S. X. Luo, Y. C. Wang, W. K. Wei, and C. G. Li, "Model tests for mechanical response of bedding rock slope under different rainfall conditions," *Chinese Journal of Rock Mechanics and Engineering*, vol. 33, pp. 755–762, 2014.

[9] Z. Li, Y. J. He, H. F. Xu, and Y. Yang, "Model test study on landslide under antecedent rainfall," *Journal of Hohai University (Natural Sciences)*, vol. 44, pp. 400–405, 2016.

[10] R. K. Regmi, K. Jung, H. Nakagawa, and J. Kang, "Study on mechanism of retrogressive slope failure using artificial rainfall," *Catena*, vol. 122, pp. 27–41, 2014.

[11] X. Q. Luo, D. F. Liu, J. Wu et al., "Model test study on landslide under rainfall and reservoir water fluctuation," *Chinese Journal of Rock Mechanics and Engineering*, vol. 24, pp. 2476–2483, 2005.

[12] Y. H. Pan, X. P. Li, L. Q. Wu, W. Wang, and F. Tan, "Model test on rainfall warning criteria of retrogressive landslide," *Journal of Yangtze River Scientific Research Institute*, vol. 33, pp. 111–115, 2016.

[13] M. Ahmadi-Adli, N. Huvaj, and N. K. Toker, "Rainfall-triggered landslides in an unsaturated soil: a laboratory flume study," *Environmental Earth Sciences*, vol. 76, no. 21, p. 735, 2017.

[14] M. S. Kim, Y. Onda, T. Uchida, J. K. Kim, and Y. S. Song, "Effect of seepage on shallow landslides in consideration of changes in topography: case study including an experimental sandy slope with artificial rainfall," *Catena*, vol. 161, pp. 50–62, 2018.

[15] D. H. Gary and T. L. Andrew, *Biotechnical Slope Protection and Erosion Control*, pp. 37–54, Van Nostrand Reinhold Company, New York, NY, USA, 1982.

[16] R. Rai and B. K. Shrivastva, "Biological stabilization of mine dumps: shear strength and numerical simulation approach with special reference to Sisam tree," *Environmental Earth Sciences*, vol. 63, no. 1, pp. 177–188, 2011.

[17] L. Dupuy, T. Fourcaud, and A. Stokes, "A numerical investigation into the influence of soil type and root architecture on tree anchorage," *Plant and Soil*, vol. 278, no. 1-2, pp. 119–134, 2005.

[18] L. Dupuy, T. Fourcaud, and A. Stokes, "A numerical investigation into factors affecting the anchorage of roots in tension," *European Journal of Soil Science*, vol. 56, no. 3, pp. 319–327, 2005.

[19] G. Wang, W. Li, P. Wang, X. Yang, and S. Zhang, "Deformation and gas flow characteristics of coal-like materials under triaxial stress conditions," *International Journal of Rock Mechanics and Mining Sciences*, vol. 91, pp. 72–80, 2017.

[20] M. Burylo, C. Hudek, and F. Rey, "Soil reinforcement by the roots of six dominant species on eroded mountainous manly slopes (Southern Alps, France)," *Catena*, vol. 84, no. 1-2, pp. 70–78, 2011.

[21] P. Voottipruex, D. T. Bergado, W. Mairaeng, S. Chucheepsakul, and C. Modmoltin, "Soil reinforcement with combination roots systems: a case study of vetiver grass and acacia mangium wild," *Lowland Technology International the Official Journal of the International Association of Lowland Technology*, vol. 10, pp. 56–67, 2008.

[22] M. Saifuddin and N. Osman, "Evaluation of hydro-mechanical properties and root architecture of plants for soil reinforcement," *Current Science*, vol. 107, no. 5, pp. 845–852, 2014.

[23] G. B. Bischetti, E. A. Chiaradia, T. Simonato et al., "Root strength and root area ratio of forest species in Lombardy (Northern Italy)," *Plant and Soil*, vol. 278, no. 1-2, pp. 11–22, 2005.

[24] M. Genet, A. Stokes, T. Fourcaud, and J. E. Norris, "The influence of plant diversity on slope stability in a moist evergreen deciduous forest," *Ecological Engineering*, vol. 36, no. 3, pp. 265–275, 2010.

[25] G. Zhang, J. Y. Qian, R. Wang, and J. M. Zhang, "Centrifuge model test study of rainfall-induced deformation of cohesive soil slopes," *Soils and Foundations*, vol. 51, no. 2, pp. 297–305, 2011.

[26] W. J. Zhang and K. Maeda, "The model test and SPH simulations for slope and levee failure under heavy rainfall considering the coupling of soil, water and air," *Geo-Shanghai*, vol. 236, pp. 538–547, 2014.

[27] W. Q. Luo, F. A. Li, X. S. Liu, and L. Huang, "Evolution stage division of landslide based on analysis of multivariate time series," *Earth Science*, vol. 41, pp. 711–717, 2016.

[28] J. X. Ding, Y. J. Shang, Z. F. Yang, and L. Q. Zhang, "New method of predicting rainfall-induced landslides," *Chinese Journal of Rock Mechanics and Engineering*, vol. 23, pp. 3738–3743, 2004.

[29] H. Fukuda and T. W. Chou, "A probabilistic theory of the strength of short-fiber composites with variable fiber length and orientation," *Journal of Materials Science*, vol. 17, no. 4, pp. 1003–1011, 1982.

[30] L. Yang, H. X. Wang, C. P. Han, H. Guo, Y. F. Gong, and Y. L. He, "Research on the strength variation of root-clay systems under freeze-thaw action," *Advances in Materials Science and Engineering*, vol. 2017, Article ID 5853034, 14 pages, 2017.